Surface & Coatings Technology 496 (2025) 131716

Contents lists available at ScienceDirect

Surface & Coatings Technology

journal homepage: www.elsevier.com/locate/surfcoat

High-loading 316L stainless steel by integrated low-temperature surface nitriding and DLC deposition

Xiang Zhang [a], Yaoyao Liu [b], Ziqi Ma [a], Shusheng Chen [a], Minyu Ma [a], Dongjie Yang [a], Xiaokai An [a], Yanfei Zhao [b], Lingjie Chen [b], Liangliang Liu [a,c,d,e,*], Ricky K.Y. Fu [c,d,e], Paul K. Chu [c,d,e], Zhongzhen Wu [a,**]

[a] School of Advanced Materials, Peking University Shenzhen Graduate School, Shenzhen 518055, China
[b] National Key Laboratory of Marine Corrosion and Protection, Luoyang Ship Material Research Institute, 471023, China
[c] Department of Physics, City University of Hong Kong, Tat Chee Avenue, Kowloon, Hong Kong, China
[d] Department of Materials Science and Engineering, City University of Hong Kong, Tat Chee Avenue, Kowloon, Hong Kong, China
[e] Department of Biomedical Engineering, City University of Hong Kong, Tat Chee Avenue, Kowloon, Hong Kong, China

ARTICLE INFO

Keywords:
316L
High loading
Low temperature nitriding
DLC coating

ABSTRACT

Because of the low hardness of 316L stainless steel, enhancing its surface hardness and wear resistance by coating technologies often produces the "egg-shell effect," resulting in suboptimal coating performance. Although nitriding is an effective method to improve the load-bearing capacity of soft substrates like 316L stainless steel, the high nitriding temperature tends to produce Cr compounds, which deteriorates the corrosion resistance. To address this issue, we describe a novel approach that couples arc-enhanced plasma nitriding with high-energy pulsed biasing to achieve high-efficiency, low-temperature nitriding. Our results indicate that the application of kV-level pulsed bias enables rapid nitriding at a low temperature (400 °C) and a nitriding rate of up to 6.5 μm/h. The nitrided layer consists mainly of the γ-N phase without showing the formation of Cr compounds. The hardness of the nitriding layer of 1300 HV provides sufficient bearing capacity for the subsequent deposition of a diamond-like carbon (DLC) layer. The integrated nitriding/DLC-processed substrate shows a low wear rate of 2.55×10^{-16} m^3/N·m even at ultra-high contact stress of 3.88 GPa. Furthermore, wear resistance is enhanced by nearly 36 times compared to the standalone DLC coating.

1. Introduction

316L stainless steel is widely used in medical devices due to its excellent corrosion resistance, satisfactory biocompatibility, and cost-effectiveness [1,2]. However, 316L suffers from significant wear during use because of low hardness, which compromises its service life. Although coating technologies theoretically can reduce wear and extend the lifespan [3,4], the low hardness of 316L prevents it from effectively supporting the coating under heavy loads and spurs the "egg-shell" effect [5,6], which adversely affects the performance of the deposited coating.

To enhance the coating load-bearing capacity of soft substrates like 316L stainless steel, nitriding is a viable technique to increase the surface hardness [7–11]. However, high-temperature nitriding tends to produce CrN/Cr_2N phases on the surface, which can reduce the corrosion resistance of stainless steel [12,13]. When the nitriding temperature is below 450 °C, the nitrided layer consists predominantly of the γ_N phase (expanded austenite, S phase), which can achieve high hardness and excellent corrosion resistance [14]. As a result, researchers have been exploring low-temperature nitriding processes such as plasma-enhanced nitriding [15,16]. In plasma nitriding, the concentration of nitrogen ions increases, and the bias voltage boosts the ion energy to improve the activity and reduce the nitriding temperature. Conventional plasma nitriding methods include active screen plasma nitriding (ASPN) [17], hollow cathode discharge nitriding(HCDN) [18], and arc-enhanced plasma nitriding(AEPN) [19]. However, ASPN and HCDN are often work at high pressure (>200 Pa) [20–22], which is much higher than that used in common PVD processes, posing challenges to the integration of nitriding and coating technologies together. In addition, at temperatures below 450 °C, their nitriding rate decreases

* Correspondence to: L. Liu, Department of Physics, City University of Hong Kong, Tat Chee Avenue, Kowloon, Hong Kong, China.
** Corresponding author.
E-mail addresses: liull620@163.com (L. Liu), wuzz@pkusz.edu.cn (Z. Wu).

https://doi.org/10.1016/j.surfcoat.2024.131716
Received 27 October 2024; Received in revised form 17 December 2024; Accepted 26 December 2024
Available online 27 December 2024

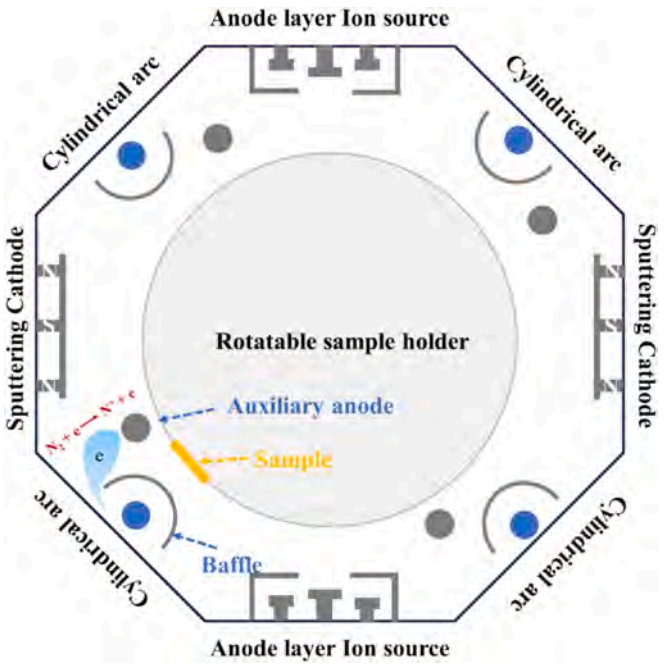

Fig. 1. Schematic diagram of the integrated nitriding/coating depositing system.

significantly to below 1 μm/h [20,23,24]. AEPN has great potential due to its high plasma density and the ability to operate at similar pressure as conventional PVD [25]. However, it is still challenging to lower the nitriding temperature to 450 °C [26,27]. Increasing the ion energy has been reported to increase the nitriding rate and reduce the nitriding temperature [28], but a high ion energy raises the substrate temperatures. For example, when the nitriding bias is below −600 V (DC or pulsed DC), the nitriding temperature still rises to >500 °C [29]. Nitriding aided by ion implantation using a pulsed bias of >10 kV can achieve high energy without raising the temperature substantially. However, the nitriding rate remains low because of the short bias duration. To address the issue, Liu et al. have proposed kV-level pulsed biasing in preparing DLC coatings at a compromised temperature and efficiency [30,31], suggesting that nitriding at a low temperature is possible.

Herein, rapid nitriding of 316L stainless steel is accomplished by generating high-density nitrogen ions using arc discharge in conjunction with kV pulsed biasing (~3 kV, 8 % duty cycle). Although the nitriding temperature is between 380 and 400 °C, a high nitriding rate of 6.5 μm/h is accomplished. The nitrided layer consists primarily of the γ-N phase, and no Cr compounds is formed. The combined nitriding/DLC deposition process significantly enhances the load-bearing capacity of the stainless-steel substrate and improves the adhesion strength of the DLC. Even under very high cyclic loadings, excellent protective effects are observed, as exemplified by wear resistance improvement of nearly 36 times compared to a standalone DLC coating.

2. Experimental details

The substrate was polished 316L stainless steel (30 × 30 × 1 mm^3). The substrates were polished sequentially using 320#, 600#, 1000#, 1500#, and 3000# SiC papers, followed by final polishing with gold velvet and 0.5 μm diamond polishing suspension to achieve a mirror-like

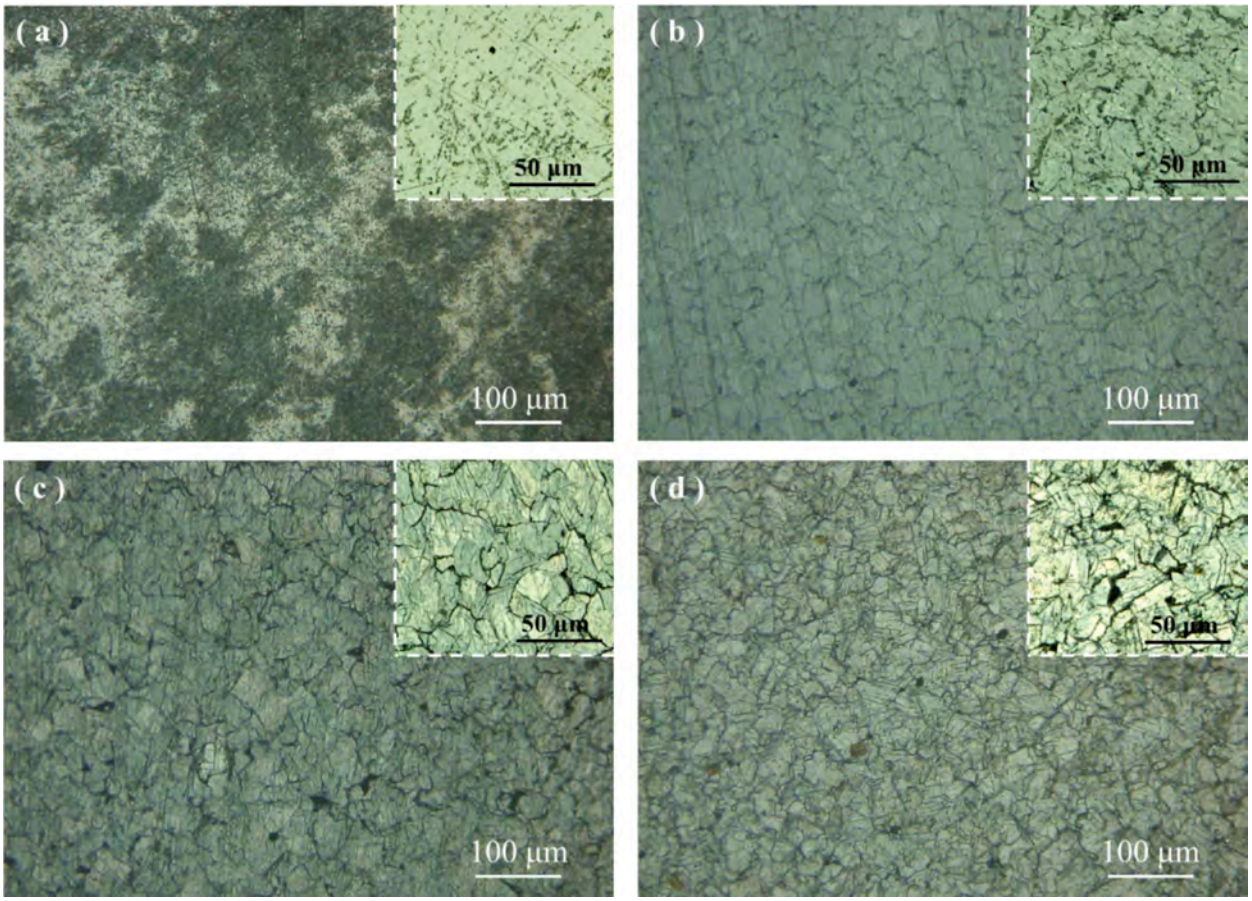

Fig. 2. Optical surface morphology of the samples after nitriding for different time periods: (a) 0 h, (b) 1 h, (c) 3 h, and (d) 5 h.

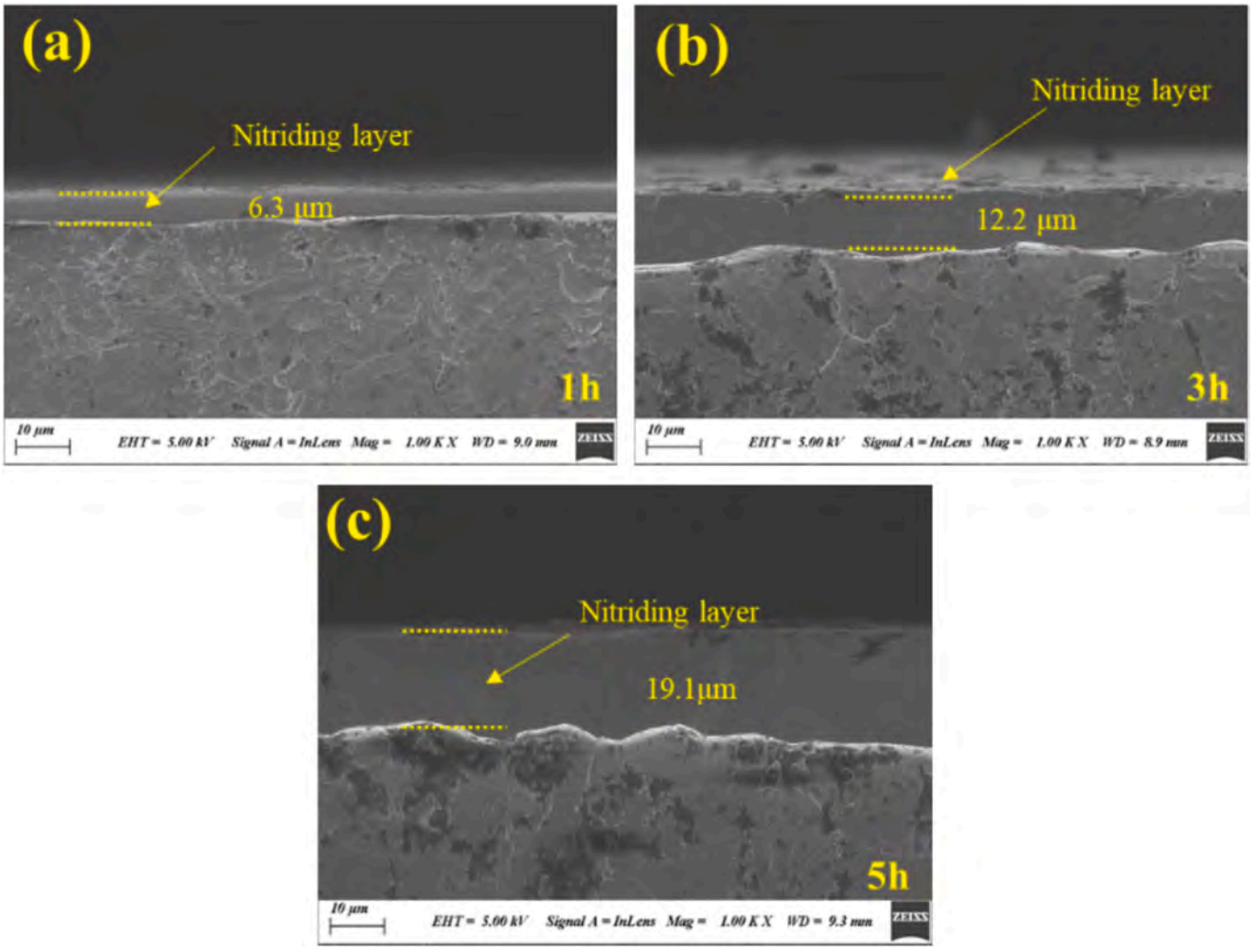

Fig. 3. Cross-sectional morphology of the samples after nitriding for different time periods.

finish. After polishing, they were cleaned ultrasonically in anhydrous ethanol for 20 min and dried with compressed air. Plasma nitriding and DLC deposition were carried out in a custom vacuum chamber (Origin S01, Shenzhen Origin-Vac Lab., China) with an inner diameter of 1 m and a height of 1.2 m. The chamber was equipped with arc sources, magnetron sputtering cathodes, and an anode layer ion source. During arc-enhanced plasma nitriding, the arc shutters were closed to avoid cross-contamination and auxiliary anodes were used to attract electrons. High-density electrons ionize nitrogen and ammonia gases on the way to the auxiliary anode, forming nitrogen ions that were accelerated toward the substrate under the pulsed kV bias to achieve nitriding. The nitriding process is illustrated in Fig. 1. During nitriding, the nitriding temperature is controlled between 380 and 400 °C. A Ti target (⌀70 mm × 1000 mm) was used for arc discharge, with an arc current of 120 A, auxiliary anode current of 100 A, argon gas flow rate of 120 sccm, nitrogen gas flow rate of 120 sccm, ammonia gas flow rate of 90 sccm, and pressure of 2 Pa. The pulsed −3 kV bias was applied to the substrate with a duty cycle of 8 %, pulse width of 100 μs, and frequency of 800 Hz. The nitriding durations were 1, 3, and 5 h. After nitriding, the heating system was closed and high-power impulse magnetron sputtering (HiPIMS) was employed to deposit a Cr/CrCx/CrC transition layer in an Ar/C_2H_2 atmosphere using a Cr target (530 × 100 × 6 mm^3). The Ar flow rate was 120 sccm, and the maximum C_2H_2 flow rate was 80 sccm. The HiPIMS discharge parameters were: 750 V, 50 Hz, and 300 μs. The Cr layer was deposited at a DC bias of −700 V for 2 min, after which the bias was reduced to −100 V. The acetylene flow rate was raised linearly to 80 sccm for 6 min to deposit CrCx, followed by CrC deposition for 2 min at a steady 40 sccm C_2H_2 flow rate. After completing the transition layer deposition, a DLC coating was deposited using the anode layer ion source. The ion source power was maintained at 1 kW, and the argon and C_2H_2 flow rates were 120 sccm and 90 sccm, respectively. Deposition was carried out for 3 h at a temperature of about 95 °C. A high-energy pulsed bias (7.5 kV, 50 Hz, and 100 μs) was applied to enhance the film density and reduce stress during deposition.

The morphology and composition of the coatings were characterized by field-emission scanning electron microscopy (FE-SEM, ZEISS SUPRA® 55) and energy-dispersive X-ray spectrometry (EDS, Oxford X-Max 20), respectively. Before observation, the samples were corroded by Marble reagent, which is consist by hydrochloric acid 20 mL, water 20 mL and copper sulfate 5 g. The structure of the nitrided layer and coatings was determined by Grazing Incidence X-ray Diffraction at incidence angle of 1° and step length of 0.03° (GIXRD, Bruker D8) and Raman scattering (Horiba LabRam HR VIS). The hardness was measured under different loads on the micro-nano indenter (Fisherscope HM2000) and microhardness tester. The adhesion strength was evaluated by the scratch test using linearly increasing loads from 0 N to 100 N at a rate of 10 N/mm. The surface roughness of the coatings was assessed on the DEKTAK XT profilometer. The tribological test was conducted on a ball-on-disk tribometer (Rtec MFT-5000) under loads of 50 N and 100 N with a sliding speed of 6.28 m/min. The counterpart was a 4 mm diameter

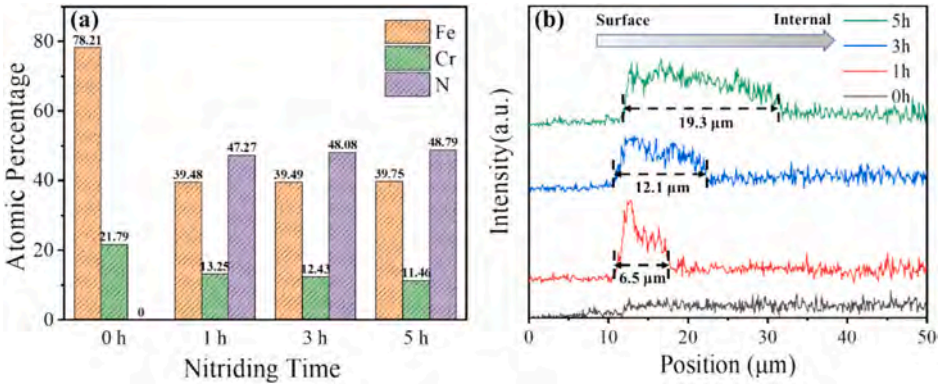

Fig. 4. Surface elemental composition and cross-sectional line scans of the nitrided layer by EDS.

Si3N4 ball. The rotational diameter and test duration were 10 mm and 2 h, respectively. The wear rate was calculated based on the corresponding wear volume by the following equation [32]:

$$K = \upsilon/sF$$

where K is the wear rate, υ is the wear volume in m^3, s is the total sliding distance in meters, and F is the applied normal force in Newton.

3. Results and discussion

Fig. 2 depicts the optical surface images of both the pristine and nitrided samples. The surface of the untreated sample (0 h nitriding) exhibits dark gray and light gray areas arising from the poor corrosion resistance in the metallographic etchant (copper sulfate and hydrochloric acid). The magnified metallographic micrographs in the insets reveal that the surface is flat and lacks noticeable texture. After nitriding samples (1 h, 3 h, and 5 h), microcracks appear from the surface. As the nitriding duration increases, striated protrusions become more pronounced, likely caused by the etching of grain boundaries during ion sputtering. In addition, infiltration of nitrogen ions would also leading to plastic deformation of the surface because of surface stress changes, which may also attribute the striated protrusion formation [33]. The insets also show that with increasing nitriding time, the structure remains uniform, similar to that of the non-nitrided sample, without the formation of precipitated phases.

Fig. 3 shows the cross-sectional morphologies of the samples after nitriding for 1 h, 3 h, and 5 h. The nitrided layer thicknesses are approximately 6.3 μm for the 1 h sample, 12.2 μm for the 3 h sample, and 19.1 μm for the 5 h sample, corresponding to nitriding rates of 6.3 μm/h, 4.1 μm/h, and 3.8 μm/h, respectively. Traditional nitriding rate primarily depends on the concentration gradient of N species and the reaction temperature. However, to plasma enhance nitriding, it also depends on the reactivity and the energy of N particles. In this study, arc-enhanced discharge provides a very high concentration of electrons and subsequent high ionization of nitrogen which increase the reactivity. Additionally, kilovolt-level bias gives enough energy to the N ions. Both increase in reactivity and energy improve nitriding rate to 6.5 μm/h at low temperature. The nitriding rates show a decreasing trend because nitrogen readily diffuses into the surface layer, forming a high concentration and providing a strong driving force for inward diffusion. As the thickness increases, nitrogen penetration is mitigated, as demonstrated by the decreasing nitriding rate. The cross-sectional morphology shows homogeneous contrast without precipitated phases, indicating improved corrosion resistance for Marble Reagent. The cross-sectional EDS mapping (Figs. S1 and S2 in the Supplementary Material) shows a homogeneous distribution of the Cr and Fe in the substrate and nitriding layer, indicting no Cr compounds formation and Cr segregation.

Fig. 4(a) shows that Fe, Cr, and N have relatively stable distributions in the coating with atomic concentrations of 39.5 %, 12.5 %, and 48 %, respectively. The stability in composition is primarily due to the high thickness of the nitrided layer. During high-energy nitriding, the surface composition may have already stabilized, resulting in no significant compositional differences between the different nitrided samples. The EDS line scans across the cross-section are shown in Fig. 4(b). According to the nitrogen distributions, the nitrided layer thicknesses of the 1 h, 3 h, and 5 h samples are 6.5 μm, 12.1 μm, and 19.3 μm, respectively, consistent with SEM. The nitrogen concentration in the 1 h decreases gradually with depth. As the nitriding time increases, a higher surface nitrogen concentration and nitrogen plateau are observed due to nitrogen ion implantation at the applied bias explained by the trapping–detrapping model [34], concentration-dependent diffusion model [35] and a combination of the two models [36]. The core mechanism is the strong affinity between Cr and N in austenitic stainless steel. Only when Cr—N bonding is saturated does nitrogen diffuse further inward, giving rise to the formation of this concentration plateau.

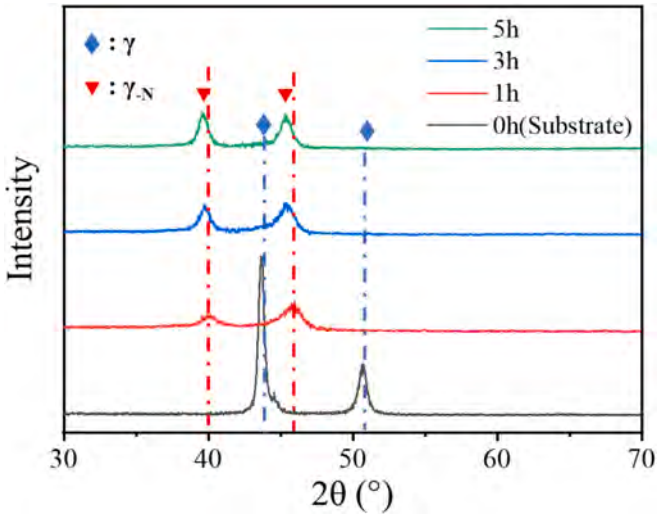

Fig. 5. GIXRD spectra of samples nitrided for different time periods.

Fig. 5 shows the XRD patterns of the samples after nitriding. The untreated substrate exhibits a strong primary peak at 44.2°, corresponding to the γ-phase of austenitic stainless steel. In the 1 h sample, additional peaks at 40.1° and 45.1° corresponding to the (111) and (200) planes of the γ_N phase emerge [37]. As the nitriding time increases to 3 and 5 h, the intensity of the diffraction peaks increases, and the peaks shift slightly to smaller angles indicative of lattice expansion [38]. This is primarily due to the increased nitrogen solubility in the lattice, consistent with EDS. The formation of the single γ-N phase is mainly due to the low nitriding temperature, which prevents the formation of Cr compounds.

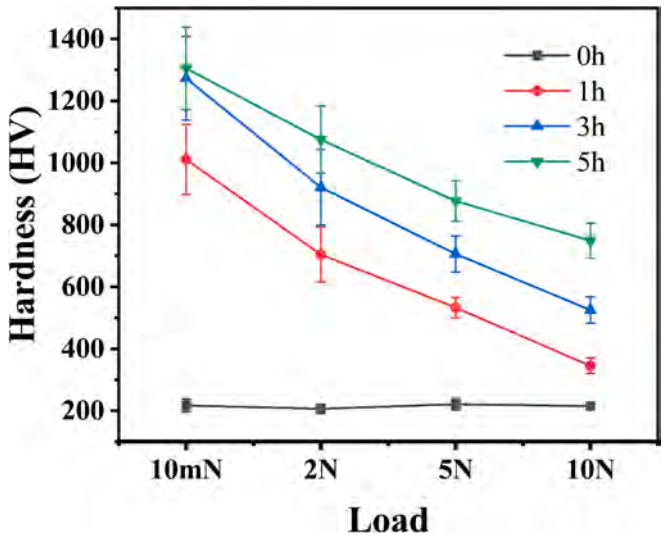

Fig. 6. Hardness under different loads after nitriding.

To evaluate the effects of the nitride layer thickness on the load-bearing capacity, hardness measurements are conducted under different loads, as shown in Fig. 6. The substrate hardness remains stable between 210 and 220 HV, with minimal influence from the applied load. The hardness of the samples nitrided for 1 h, 3 h, and 5 h under 10 mN is 1000 HV, 1250 HV, and 1300 HV, respectively. As the load increases, the hardness decreases. However, under the same load, the sample nitride for a longer time shows higher hardness, and the rate of hardness reduction decreases with increasing load. This phenomenon is mainly attributed to the thicker nitrided layer formed during long-time nitriding, which enhances the load-bearing capacity under indentation and reduces the influence of the underlying layer. Consequently, even when the load is increased to 10 N, the hardness of the 3 h and 5 h samples remain at 530 HV and 750 HV, respectively.

To investigate the effects of the nitrided layer on improving the "eggshell effect", Cr/CrCx/CrC/DLC coatings are deposited directly on the untreated substrate and nitrided samples after nitriding. Fig. 7 shows that the total coating thickness is approximately 3.5 μm, including a 0.8 ± 0.1 μm thick Cr/CrCx/CrC transition layer (bright region) and a 2.7 ± 0.2 μm thick DLC layer. No obvious porosity is observed from the Cr/CrCx/CrC/DLC coating and nitrided surface, indicating good adhesion.

The surface roughness of the samples before and after DLC deposition is measured. As shown in Fig. 8, the surface roughness (Ra) of the substrate is approximately 0.11 μm. With increasing nitriding time, it increases gradually to 0.13 μm and 0.16 μm, and the 5 h sample shows a surface roughness of 0.24 μm, which is slightly lower than samples with similar thickness by other nitriding methods [10,11,23]. After DLC deposition, the surface roughness of all samples, except for the untreated one, decreases on account of the filling of surface depressions of the PVD coating during deposition [39].

The structure of the composite Cr/CrCx/CrC/DLC coating is characterized by X-ray diffraction (XRD) and Raman scattering, as shown in Fig. 9. The change of the XRD patterns is consistent with that observed before coating deposition. However, a small broad peak appears at 44° from the underlying Cr/CrCx/CrC transition layer. All the samples exhibit asymmetrical broad peaks in the range of 1000–1800 cm^{-1} characteristic of DLC in the Raman spectra, including the D peak at 1350 cm^{-1} and G peak at 1580 cm^{-1} [40]. The ratio of I_D/I_G indicates the proportion of sp^2 to sp^3 bonding in the coating. Specifically, a smaller I_D/I_G ratio suggests more sp^3 [41]. Peak fitting reveals that the I_D/I_G ratio of all the samples is approximately 0.547, which is relatively low and indicates a higher proportion of sp^3 and greater hardness. Moreover, there is no difference among the various samples, implying that the surface nitriding layer does not affect the deposition of subsequent coatings.

Hardness tests are conducted after DLC deposition, as shown in Fig. 10. Under a load of 10 mN, the hardness is around 1850 HV. The hardness measured under small loads predominantly reflects the hardness of the surface DLC layer. The consistent sp^3 content of the DLC coating, as indicated by the Raman results in Fig. 9, leads to a uniform

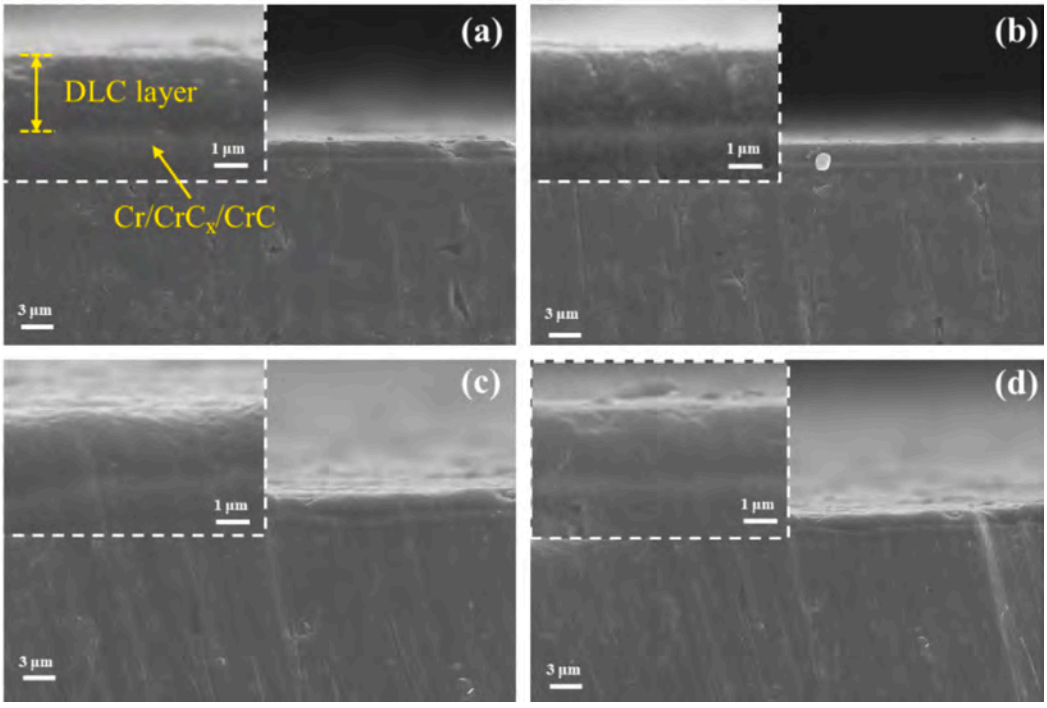

Fig. 7. Cross-sectional morphology of the samples after nitriding for different time durations after DLC deposition: (a) Without nitriding; (b) 1 h nitriding; (c) 3 h nitriding and (d) 5 h nitriding.

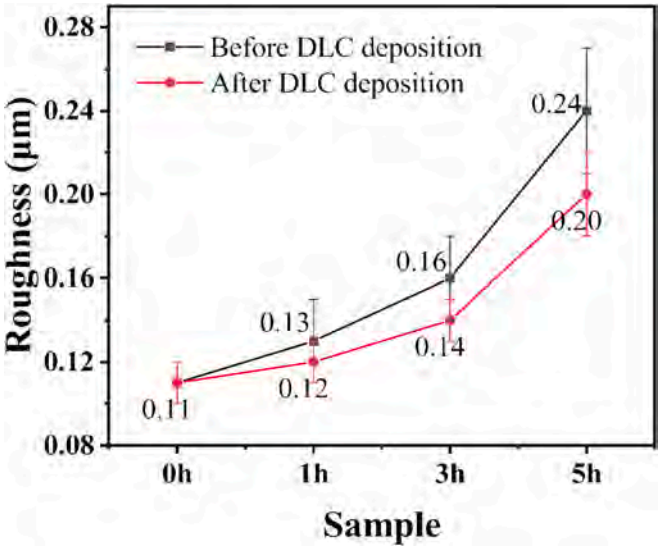

Fig. 8. Surface roughness of the samples before and after DLC deposition.

hardness value of approximately 1850 HV. When the load is increased to 2 N, the hardness of the untreated sample drops to 400 HV, which approaches the substrate hardness, indicating that the substrate does not provide adequate support for the coating. In contrast, the hardness of the nitrided samples under 2 N decreases only slightly, with the reduction in hardness becoming less pronounced with nitriding time. When the load is further increased to 5 N, a significant drop in hardness is observed. However, the hardness of the 3 h and 5 h nitrided samples is about 900 HV. Upon further increase of the load to 10 N, the hardness of the 3 h and 5 h samples is 600 HV and 880 HV, respectively, indicating that the nitrided layer provides good load-bearing capacity.

The adhesion strength of coatings is important. Fig. 11 depicts the morphology after the scratch test. The untreated sample exhibits a metallic color at the scratch onset, indicative of coating delamination. The adhesion strength is approximately 29 N. With regard to the 1 h and 3 h samples, whitening occurs closer to the rear end of the scratch, revealing improved adhesion strength of 61 N and 73 N, respectively. The adhesion is higher than most of the integrated Nitriding/DLC coatings, which is mostly between 20 and 40 N [9,10]. The improved adhesion can be ascribed to the dense nitrided surface, high ionization rate in HiPIMS, direct deposition after nitriding, and prevention of secondary contamination. However, the adhesion strength of the 5 h nitrided sample decreases to 50 N. The adhesion strength is primarily related to stress in the coating and the interface with the substrate. In this study, the PVD coating preparation process is the same, and the theoretical adhesion strength should be comparable. However, previous research reveals that the adhesion increases linearly with the increasing of substrate hardness in scratch test [42]. During the scratch test, coating failure is primarily associated with the tangential force [43], which is influenced by the indentation depth and surface roughness of the coating [10]. As for the untreated sample, the softer substrate allows for greater indentation under the same load, even penetration to the substrate, resulting in a very high tangential force and making the coating

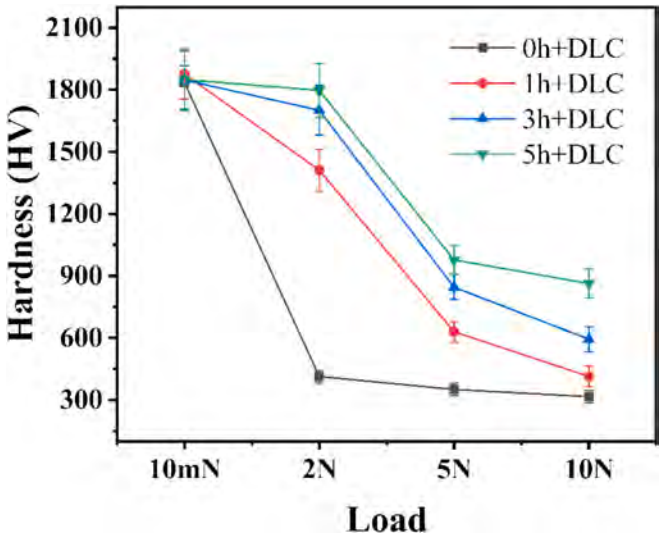

Fig. 10. Hardness under different loads after DLC deposition on the nitrided surface.

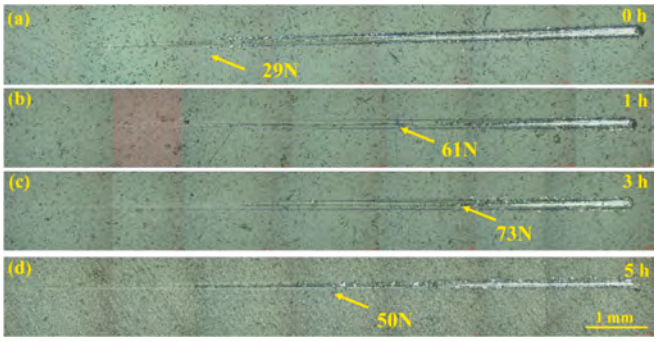

Fig. 11. Scratch morphology of different samples.

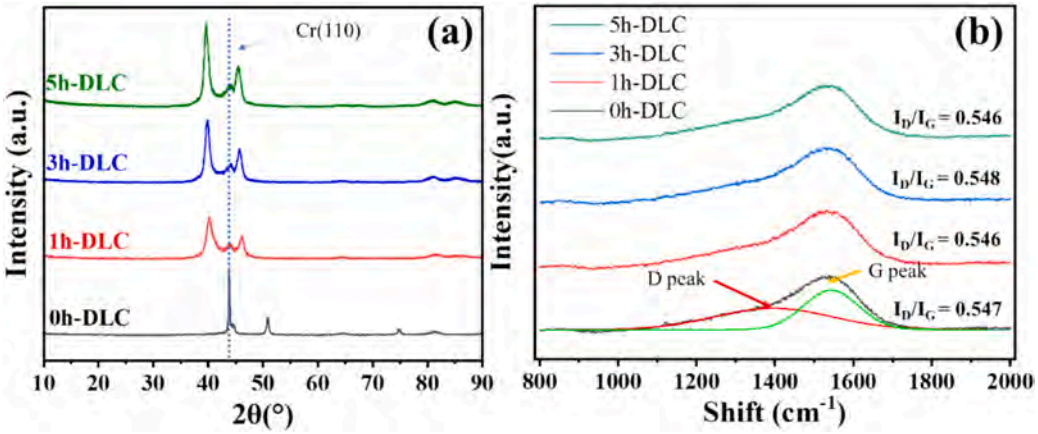

Fig. 9. XRD and Raman spectra of different samples after DLC deposition.

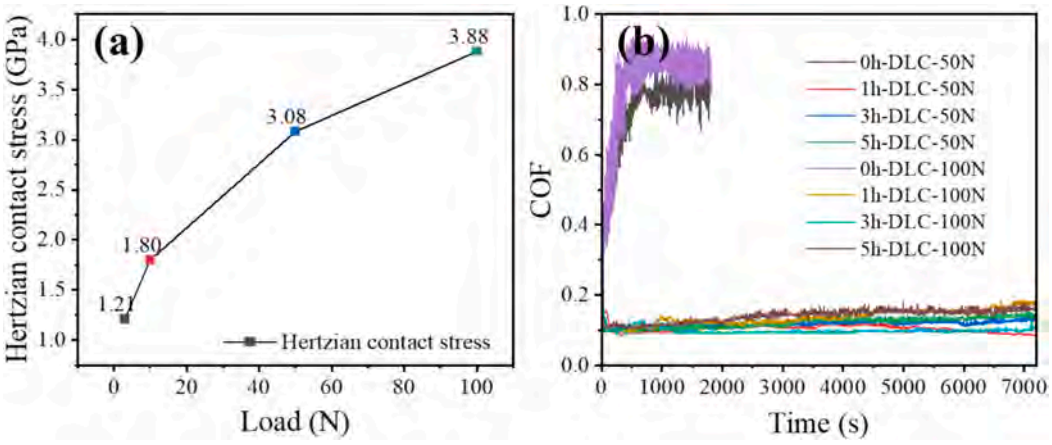

Fig. 12. (a) Hertzian contact stress under different loads and (b) friction coefficients of different samples under 50 N and 100 N loads.

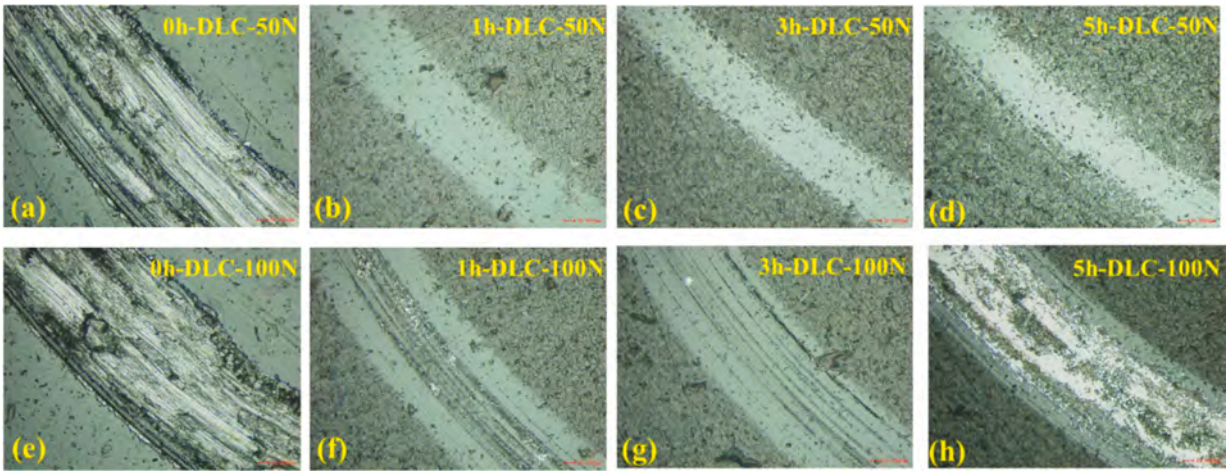

Fig. 13. Morphology of wear tracks on different samples.

prone to delamination. When the substrate hardness is higher, both the substrate and coating deform less under the same load, resulting in a lower tangential force, which only increases at larger loads. Consequently, the nitrided samples have greater adhesion strength. In addition, Ma S.L. et al. found short nitriding time could also reduce the residual stress of the coatings [44], which could also attribute to the adhesion improvement with nitriding. However, as the nitriding time is further extended, the surface roughness increases and the adhesion decline, which is consisted with the results from A. Nishimoto [10]. The larger protrusions appeared in samples with longer nitriding time endure significantly high tangential forces during lateral sliding, leading to lower adhesion strength. Therefore, the adhesion strength of the 5 h sample declines.

To assess the extent of the mitigation of the "eggshell effect" stemming from nitriding and investigate the fatigue performance under high loads, ball-on-disc friction and wear tests are conducted using 4 mm diameter Si_3N_4 balls against the coatings under various loads. Firstly, the Hertzian contact stresses under different loads are calculated using the Hertz formula [45], as shown in Fig. 12(a). Under loads of 3 N and 10 N (standard loads), the contact stresses are 1.21 GPa and 1.80 GPa, respectively, whereas under loads of 50 N and 100 N, the contact stresses reach 3.08 GPa and 3.88 GPa. Based on these calculations, the higher contact stresses (3.08 GPa and 3.88 GPa) are selected for the fatigue wear tests. Fig. 12(b) presents the variations of the friction coefficients with time under 50 N and 100 N loads. Under the 50 N load, the untreated sample exhibits an immediate increase in friction coefficients at the start of the test, indicating instant failure under fatigue wear conditions. In contrast, the nitrided samples maintain low friction coefficients during the two-hour friction wear test, showing values of 0.11–0.13. When the load is raised to 100 N, the untreated sample again shows immediate wear failure and a severe eggshell effect. In contrast, the nitrided samples continue to exhibit low friction coefficients even under a load of 3.88 GPa. Aside from the 3 h sample, which has a low friction coefficient, the friction coefficients of the 1 h and 5 h samples increase slightly to 0.16–0.18.

To analyze the failure modes and processes during the friction and wear tests, the morphology after wear is shown in Fig. 13. Under a load of 50 N, the wear track of sample without nitriding clearly exposes the substrate and exhibits an irregular pattern with pronounced grooves, indicative of significant abrasive wear. This phenomenon is primarily attributed to the "eggshell effect," which results in the instantaneous fracture of the coating. On the other hand, the transition layer composed of Cr/CrCx/CrC acts as the abrasive medium, leading to the visible wear scar even after only 5 min. Eugenia L. D. et al. also got the similar results in the DLC coated 316L surface at similar contact stress [46]. The wear tracks of the other nitride samples (1 h-DLC-50 N, 3 h-DLC-50 N, 5 h-DLC-50 N) are smooth, showing no significant exposure of the substrate, implying that the DLC coating maintains effective protective properties under this load. Under a load of 100 N, the morphology of the non-nitrided samples resembles that under 50 N, suggesting similar failure modes, albeit more severe wear. As for the 1 h sample, bright coloration appears from the center of the wear track. However, the discontinuous

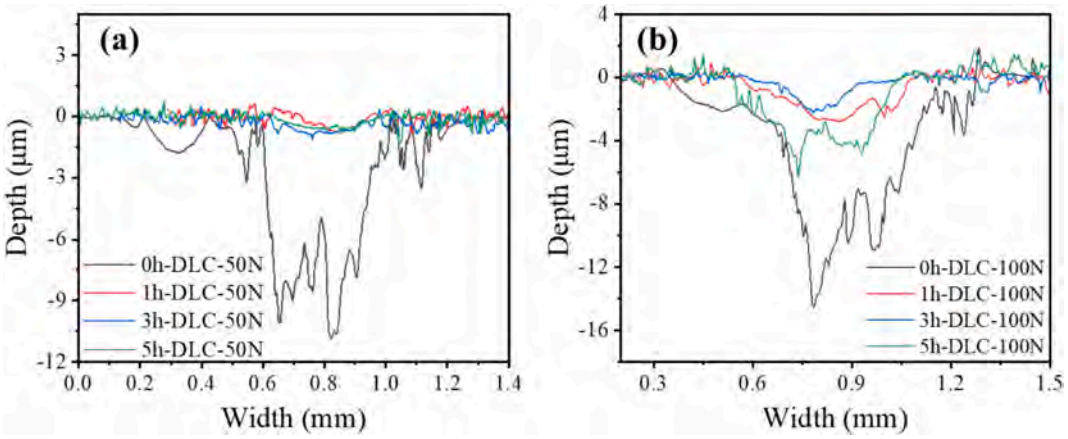

Fig. 14. Wear track profiles under different loads.

Table 1
Wear rates of the nitriding/DLC samples for different nitriding time periods.

Load/sample	Wear rate ($\times 10^{-16}$ m^3/N·m)			
	0 h	1 h	3 h	5 h
50 N	82.8	2.44	2.53	2.95
100 N	94.8	4.84	2.55	8.33

nature of brightness indicates partial wear-through of the DLC layer. This may be because the relatively thin nitrided layer provides insufficient mitigation of the eggshell effect. The central area corresponds to the apex of the grinding ball, where deformation is maximal, resulting in more severe wear. The wear track of the samples nitrided for 3 h does not show a metallic color, suggesting effective avoidance of the eggshell effect and excellent protection. Thin grooves are observed in the wear track in Fig. 13(g), indicting abrasion wear mechanism. The rigid nitriding layer with higher hardness will increase stress concentration of the film when contacted with the Si_3N_4 ball, and the fine debris detached from the carbon film causes scratches of the film and the counter body ball, giving rise to the formation of the grooves [47]. The wear track of the samples nitrided for 5 h exhibits a bright white color. However, the scar remains relatively smooth. Coupled with a slight increase in the friction coefficients toward the end of the test, it can be inferred that wear occurs slowly rather than instantaneous failure associated with the egg-shell effect. The minor increase in friction coefficients, albeit DLC wear, may be due to wear debris providing a certain degree of lubrication. Severe wear is observed from the 5 h samples because of the larger surface roughness, and local protrusions experience significant contact stress and failure.

As shown in Fig. 14, under a load of 50 N and after 30 min, the depth of the wear track of the untreated sample reaches 10.7 μm, with the width approaching 1 mm, indicating poor wear resistance. In contrast, the other samples exhibit a wear scar depth of approximately 1 μm and a width of about 0.3 mm without penetration. Under a load of 100 N, the untreated sample shows significant depth and width approaching 15 μm and 1 mm, respectively. With regard to the sample nitrided for 1 h under a load of 100 N, the maximum wear track depth is 2.8 μm, indicative of a worn coating similar to that shown in Fig. 11. The wear track depth of the sample nitrided for 3 h is 2 μm, which is less than the DLC thickness, indicating that there is no penetration. Meanwhile, the sample nitrided for 5 h displays a maximum wear track depth of approximately 6 μm, confirming that the coating is also worn. The wear rates calculated from the wear scars are summarized in Table 1. As for the untreated sample under loads of 50 N and 100 N, the wear rates are 82.8 $\times$ 10^{-16} m^3/N·m and 94.8 $\times$ 10^{-16} m^3/N, respectively. In comparison, under loads of 50 N and 100 N, the 1 h, 3 h, and 5 h samples exhibit no evident eggshell effect, and the wear rate decreases to 2.5 $\times$ 10^{-16} m^3/N·m, which is about 36 times less than that of the pristine sample. The wear rate for the 3 h nitride sample is much lower than the reported data in the previous researches (higher than 6.5 $\times$ 10^{-16} m^3/N·m) [9,11], which was possibly attributed to the harder nitriding layer providing enough load-bearing capacity. The results disclose that low-temperature nitriding of 316L plays a significant role in enhancing the service life of the DLC coating.

4. Conclusion

To address the issue of the eggshell effect that often occurs when depositing PVD coatings on a soft 316L substrate, arc-enhanced plasma nitriding is coupled with DLC deposition. The effects of the different nitriding depths on the eggshell effect are determined. By utilizing high-energy pulsed bias coupled with arc-enhanced plasma nitriding, rapid nitriding of 316L is accomplished at a low temperature of 400 °C with a nitriding rate of 6.5 μm/h. As a result of the low-temperature nitriding, the formation of Cr compounds is avoided. The DLC coating deposited on the nitrided surface shows enhanced bonding strength. Benefiting from the higher hardness of the nitrided layer, the DLC coating effectively prevents the eggshell effect and maintains good protective capability under a high contact stress of 3.88 GPa, consequently producing a wear rate nearly 36 times less than of the untreated substrate.

CRediT authorship contribution statement

Xiang Zhang: Writing – review & editing, Visualization, Validation. **Yaoyao Liu:** Investigation. **Ziqi Ma:** Resources. **Shusheng Chen:** Resources. **Minyu Ma:** Resources. **Dongjie Yang:** Resources, Methodology. **Xiaokai An:** Resources. **Yanfei Zhao:** Resources. **Lingjie Chen:** Resources. **Liangliang Liu:** Writing – original draft. **Ricky K.Y. Fu:** Resources. **Paul K. Chu:** Supervision. **Zhongzhen Wu:** Supervision, Project administration.

Declaration of competing interest

The authors declare that they have no known competing financial interests or personal relationships that could have appeared to influence the work reported in this paper.

Acknowledgments

This work was financially supported by the National Key Research and Development Program of China (Grant No. 2023YFA1608802), Shenzhen Science and Technology Research Plan (Grant No. KJZD20231023100304009), Sustainable Supporting Funds for Colleges

and Universities in 2022 (Grant No. 20220810143642004), National Natural Science Foundation Youth Science Fund project (Grant No. 52305174), Postdoctoral Research Fund Project (Grant No. 2024M750089), City University of Hong Kong Internal Fund for ITF Projects (Grant No. 9678148), and City University of Hong Kong Donation Research Grants (Grant Nos. DON-RMG 9229021 and 9220061).

Appendix A. Supplementary data

Supplementary data to this article can be found online at https://doi.org/10.1016/j.surfcoat.2024.131716.

Data availability

Data will be made available on request.

References

[1] L. Gil, S. Brühl, L. Jiménez, O. Leon, R. Guevara, M.H. Staia, Corrosion performance of the plasma nitrided 316L stainless steel, Surf. Coat. Technol. 201 (2006) 4424–4429, https://doi.org/10.1016/j.surfcoat.2006.08.081.
[2] A.F. Yetim, Investigation of wear behaviYr of titanium oxide films, produced by anodic oxidation, on commercially pure titanium in vacuum conditions, Surf. Coat. Technol. 205 (2010) 1757–1763, https://doi.org/10.1016/j.surfcoat.2010.08.079.
[3] L. Liu, Q. Ruan, Z. Wu, D. Li, C. Huang, Y. Wu, T. Li, Z. Wu, X. Tian, R.K.Y. Fu, P. K. Chu, Fabrication and cutting performance of CrAlN/CrAl multilayer coatings deposited by continuous high-power magnetron sputtering, Ceram. Int. 48 (2022) 14528–14536, https://doi.org/10.1016/j.ceramint.2022.01.346.
[4] L. Liu, Z. Wu, S. Cui, Abrasion and erosion behavior of DLC-coated oil-well tubings in a heavy oil/sand environment, Surf. Coat. Technol. 357 (2019) 379–383, https://doi.org/10.1016/j.surfcoat.2018.09.081.
[5] T. Fu, Z.F. Zhou, Y.M. Zhou, X.D. Zhu, Q.F. Zeng, C.P. Wang, K.Y. Li, J. Lu, Mechanical properties of DLC coating sputter deposited on surface nanocrystallized 304 stainless steel, Surf. Coat. Technol. 207 (2012) 555–564, https://doi.org/10.1016/j.surfcoat.2012.07.076.
[6] J.C. Avelar-Batista, E. Spain, G.G. Fuentes, A. Sola, R. Rodriguez, J. Housden, Triode plasma nitriding and PVD coating: a successful pre-treatment combination to improve the wear resistance of DLC coatings on Ti6Al4V alloy, Surf. Coat. Technol. 201 (2006) 4335–4340, https://doi.org/10.1016/j.surfcoat.2006.08.070.
[7] T. Morita, A. K, H. S, Effect of hybrid surface treatment composed of plasma nitriding and DLC coating on friction coefficient and fatigue strength of stainless steel, Mater. Trans. 661 (2013) 105–114, https://doi.org/10.2320/matertrans.M2012426.
[8] A.F. Yetim, M.Y. Codur, M. Yazici, Using of artificial neural network for the prediction of tribological properties of plasma nitrided 316L stainless steel, Mater. Lett. 158 (2015) 170–173, https://doi.org/10.1016/j.matlet.2015.06.015.
[9] E.L. Dalibón, R.D. Moreira, D. Heim, C. Forsich, S.P. Brühl, Soft and thick DLC deposited on AISI 316L stainless steel with nitriding as pre-treatment tested in severe wear conditions, Diam. Relat. Mater. 106 (2020) 107881, https://doi.org/10.1016/j.diamond.2020.107881.
[10] A. Nishimoto, R. Amano, T. Tamiya, Duplex treatment of active screen plasma nitriding and amorphous hydrogenated carbon coating, Appl. Surf. Sci. Adv. 6 (2021) 100129, https://doi.org/10.1016/j.apsadv.2021.100129.
[11] Y. Uzun, Tribocorrosion properties of plasma nitrided, Ti-DLC coated and duplex surface treated AISI 316L stainless steel, Surf. Coat. Technol. 441 (2022) 128587, https://doi.org/10.1016/j.surfcoat.2022.128587.
[12] T. Khan, Y. Tamura, H. Yamamoto, A. Morina, A. Neville, Investigation of the tribological and tribochemical interactions of different ferrous layers applied to nitride surfaces, J. Tribol. 143 (2021), https://doi.org/10.1115/1.4047588.
[13] Y. Cheng, Z. Wang, Research of the wear resistance of 35CrMoA steel in laser quenching/nitrided layer, in: Proceedings of 2011 International Conference on Electronic & Mechanical Engineering and Information Technology, IEEE, 2011, pp. 3457–3460, https://doi.org/10.1109/EMEIT.2011.6023067.
[14] Z. Zhang, T. Bell, Structure and corrosion resistance of plasma nitrided stainless steel, Surf. Eng. 1 (1985) 131–136, https://doi.org/10.1179/sur.1985.1.2.131.
[15] A. Leyland, K.S. Fancey, A.S. James, A. Matthews, Enhanced plasma nitriding at low pressures: a comparative study of d.c. and r.f. techniques, Surf. Coat. Technol. 41 (1990) 295–304, https://doi.org/10.1016/0257-8972(90)90140-8.
[16] L. Fonseca Oliveira, V. Velho De Castro, M.A. Zen Vasconcellos, J.C. Klein Das Neves, C. de Fraga Malfatti, A. Da Silva Rocha, Effects of gas mixture on active screen plasma nitriding and post-oxidation of a 4140 steel, Surf. Coat. Technol. 476 (2024) 130272, https://doi.org/10.1016/j.surfcoat.2023.130272.
[17] Y. Hoshiyama, R. Mizobata, H. Miyake, Mechanical properties of austenitic stainless steel treated by active screen plasma nitriding, Surf. Coat. Technol. 307 (2016) 1041–1044, https://doi.org/10.1016/j.surfcoat.2016.07.032.
[18] C. Alves, C.L.B. Guerra Neto, G.H.S. Morais, C.F. Da Silva, V. Hajek, Nitriding of titanium disks and industrial dental implants using hollow cathode discharge, Surf. Coat. Technol. 194 (2005) 196–202, https://doi.org/10.1016/j.surfcoat.2004.10.009.
[19] A. de Frutos, M.A. Arenas, G.G. Fuentes, R.J. Rodríguez, R. Martínez, J.C. Avelar-Batista, J.J. de Damborenea, Tribocorrosion behaviour of duplex surface treated AISI 304 stainless steel, Surf. Coat. Technol. 204 (2010) 1623–1630, https://doi.org/10.1016/j.surfcoat.2009.10.039.
[20] A. Nishimoto, T. Fukube, T. Tanaka, Effect of surface deposits on nitriding layer formation of active screen plasma nitriding, Mater. Trans. 57 (2016) 1811–1815, https://doi.org/10.2320/matertrans.M2016209.
[21] T. Fraczek, M. Ogorek, Z. Skuza, R. Prusak, Mechanism of ion nitriding of 316L austenitic steel by active screen method in a hydrogen-nitrogen atmosphere, Int. J. Adv. Manuf. Technol. 109 (2020) 1357–1368, https://doi.org/10.1007/s00170-020-05726-8.
[22] Z.H. Dong, S.N. Chen, Z.B. Bao, Enhanced plasma nitriding assisted by combining hollow cathode discharge with rare earth oxide particles for iron-based metals, Vacuum 221 (2024) 112935, https://doi.org/10.1016/j.vacuum.2023.112935.
[23] M. Broch, C.P. Fontoura, A.O. Lima, M.F.C. Ordoñez, I.F. Machado, C. Aguzzoli, M. C.M. Farias, Scratch response of hollow cathode radiofrequency plasma-nitrided and sintered 316l austenitic stainless steel, Coatings 14 (2024) 334, https://doi.org/10.3390/coatings14030334.
[24] F. Borgioli, A. Fossati, E. Galvanetto, T. Bacci, G. Pradelli, Glow discharge nitriding of aisi 316l austenitic stainless steel: influence of treatment pressure, Surf. Coat. Technol. 200 (2006) 5505–5513, https://doi.org/10.1016/j.surfcoat.2005.07.073.
[25] N. Chen, C. Chung, C. Chiang, K. Chen, J. He, Antimicrobial copper-containing titanium nitride coatings Co-deposited by arc ion plating/magnetron sputtering for protective and decorative purposes, Surf. Coat. Technol. 253 (2014) 83–88, https://doi.org/10.1016/j.surfcoat.2014.05.017.
[26] W. Liang, Surface modification of AISI 304 austenitic stainless steel by plasma nitriding, Appl. Surf. Sci. 211 (2003) 308–314, https://doi.org/10.1016/S0169-4332(03)00260-5.
[27] X.L. Wu, W. Zhong, N.J. Tang, H.Y. Jiang, W. Liu, Y.W. Du, Magnetic properties and thermal stability of nanocrystalline ε-Fe3N prepared by gas reduction-nitriding method, J. Alloys Compd. 385 (2004) 294–297, https://doi.org/10.1016/j.jallcom.2004.04.127.
[28] T. Hino, M. Harada, Y. Yamauchi, Y. Hirohata, Nitriding of silicon by using an electron cyclotron resonance nitrogen plasma, Surf. Coat. Technol. 108-109 (1998) 312–316, https://doi.org/10.1016/S0257-8972(98)00687-2.
[29] R. Valencia-Alvarado, A. de la Piedad-Beneitez, J. de la Rosa-Vázquez, R. López-Callejas, S.R. Barocio, O.G. Godoy-Cabrera, A. Mercado-Cabrera, R. Peña-Eguiluz, A.E. Muñoz-Castro, γ-N shift as a function of N2 content in AISI 304 nitriding, Vacuum 81 (2007) 1434–1438, https://doi.org/10.1016/j.vacuum.2007.04.020.
[30] L. Liu, Z. Wu, X. An, S. Xiao, S. Cui, H. Lin, R.K.Y. Fu, X. Tian, R. Wei, P.K. Chu, F. Pan, Excellent adhered thick diamond-like carbon coatings by optimizing hetero-interfaces with sequential highly energetic Cr and C ion treatment, J. Alloys Compd. 735 (2018) 155–162, https://doi.org/10.1016/j.jallcom.2017.11.057.
[31] X. An, Z. Wu, L. Liu, T. Shao, S. Xiao, S. Cui, H. Lin, R.K. Fu, X. Tian, P.K. Chu, F. Pan, High-ion-energy and low-temperature deposition of diamond-like carbon (DLC) coatings with pulsed kV bias, Surf. Coat. Technol. 365 (2019) 152–157, https://doi.org/10.1016/j.surfcoat.2018.08.099.
[32] Y.C. Ean, Y. Jang, J. Kim, W.L. Yun Hsien, N.J. Siambun, S. Kim, Effect of substrate bias on the tribological behavior of ta-C coating prepared by filtered cathodic vacuum arc, Int. J. Precis. Eng. Manuf. 18 (2017) 779–784, https://doi.org/10.1007/s12541-017-0093-5.
[33] Y. Teng, Y. Guo, M. Zhang, Y. Yang, Z. Huang, Y. Zhou, F. Wu, Y. Liang, Effect of Cr/CrNx transition layer on mechanical properties of CrN coatings deposited on plasma nitrided austenitic stainless steel, Surf. Coat. Technol. 367 (2019) 100–107, https://doi.org/10.1016/j.surfcoat.2019.03.068.
[34] W. Möller, S. Parascandola, T. Telbizova, R. Günzel, E. Richter, Surface processes and diffusion mechanisms of ion nitriding of stainless steel and aluminium, Surf. Coat. Technol. 136 (2001) 73–79, https://doi.org/10.1016/S0257-8972(00)01015-X.
[35] S. Mändl, B. Rauschenbach, Concentration dependent nitrogen diffusion coefficient in expanded austenite formed by ion implantation, J. Appl. Phys. 91 (2002) 9737–9742, https://doi.org/10.1063/1.1479749.
[36] T. Christiansen, K.V. Dahl, M.A.J. Somers, Nitrogen diffusion and nitrogen depth profiles in expanded austenite: experimental assessment, numerical simulation and role of stress, Mater. Sci. Technol. 24 (2008) 159–167, https://doi.org/10.1179/026708307X232901.
[37] T. Moskalioviene, A. Galdikas, J.P. Rivière, L. Pichon, Modeling of nitrogen penetration in polycrystalline AISI 316L austenitic stainless steel during plasma nitriding, Surf. Coat. Technol. 205 (2011) 3301–3306, https://doi.org/10.1016/j.surfcoat.2010.11.060.
[38] P.A. Dearnley, Corrosion wear response of S phase coated 316L, Surf. Eng. 18 (2002) 429–432, https://doi.org/10.1179/026708402225006277.
[39] M.C. Salvadori, D.R. Martins, M. Cattani, DLC coating roughness as a function of film thickness, Surf. Coat. Technol. 200 (2006) 5119–5122, https://doi.org/10.1016/j.surfcoat.2005.05.030.
[40] A. Grill, Diamond-like carbon: state of the art, Diam. Relat. Mater. 8 (1999) 428–434, https://doi.org/10.1016/S0925-9635(98)00262-3.
[41] A. Gangopadhyay, K. Sinha, D. Uy, D.G. Mcwatt, R.J. Zdrodowski, S.J. Simko, Friction, wear, and surface film formation characteristics of diamond-like carbon thin coating in valve train application, Tribol. Trans. 54 (2011) 104–114, https://doi.org/10.1080/10402004.2010.525693.
[42] C. Zhang, T. Hu, N. Zhang, Influence of substrate hardness on coating-substrate adhesion, Adv. Mater. Res. 177 (2010) 148–150, https://doi.org/10.4028/www.scientific.net/AMR.177.148.

[43] J. Xiaoyu, B. Lauke, T. Schueller, Frictional contact analysis of scratch test for elastic and elastic–plastic thin-coating/substrate materials, Thin Solid Films 414 (2002) 63–71, https://doi.org/10.1016/S0040-6090(02)00428-5.
[44] S. Ma, Y. Li, K. Xu, The composite of nitrided steel of h13 and tin coatings by plasma duplex treatment and the effect of pre-nitriding, Surf. Coat. Technol. 137 (2001) 116–121, https://doi.org/10.1016/S0257-8972(00)01073-2.
[45] J.A. Greenwood, K.L. Johnson, E. Matsubara, A surface roughness parameter in Hertz contact, Wear 100 (1984) 47–57, https://doi.org/10.1016/0043-1648(84)90005-X.
[46] E.L. Dalibon, R.D. Moreira, M.A. Guitar, et al., Influence of the substrate pre-treatment on the mechanical and corrosion response of multilayer DLC coatings, Diam. Relat. Mater. 118 (2021) 108507, https://doi.org/10.1016/j.diamond.2021.108507.
[47] T. Fu, Z.F. Zhou, Y.M. Zhou, et al., Mechanical properties of DLC coating sputter deposited on surface nanocrystallized 304 stainless steel, Surf. Coat. Technol. 207 (2012) 555–564, https://doi.org/10.1016/j.surfcoat.2012.07.076.

Supplementary Material

High-loading 316L stainless steel by integrated low-temperature surface nitriding and DLC deposition

Xiang Zhang, Yaoyao Liu, Ziqi Ma, Shusheng Chen, Minyu Ma, Dongjie Yang, Xiaokai An, Yanfei Zhao, Lingjie Chen, Liangliang Liu, Ricky K Y Fu, Paul K Chu, Zhongzhen Wu

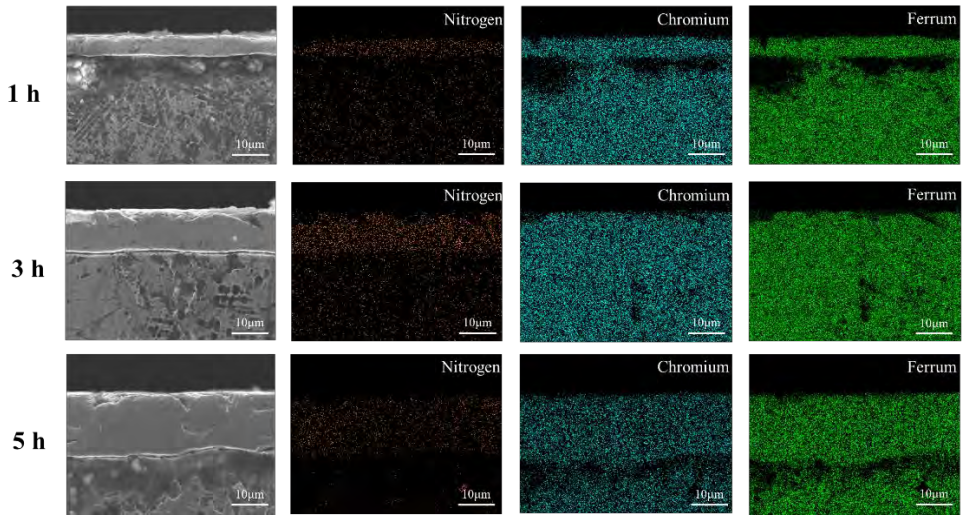

Fig.S1 The cross-sectional EDS mapping of sample nitride for different time.

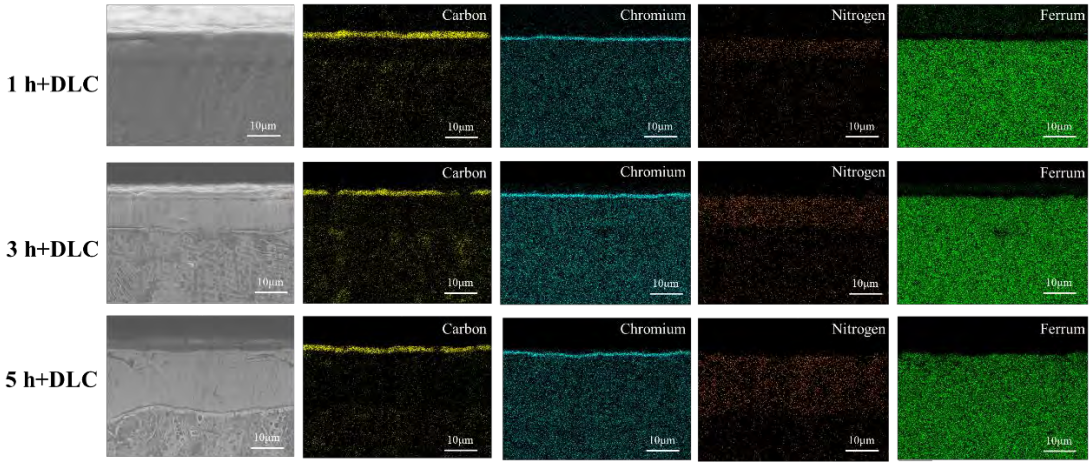

Fig.S2 The cross-sectional EDS mapping of sample nitride for different time and DLC deposition.